Hindawi
Mathematical Problems in Engineering
Volume 2017, Article ID 8945712, 11 pages
https://doi.org/10.1155/2017/8945712

Research Article

Numerical Prediction and Performance Experiment in an Engine Cooling Water Pump with Different Blade Outlet Widths

Wei Li, Xiaofan Zhao, Weiqiang Li, Weidong Shi, Leilei Ji, and Ling Zhou

Research Center of Fluid Machinery Engineering and Technology, Jiangsu University, Zhenjiang, China

Correspondence should be addressed to Wei Li; lwjiangda@ujs.edu.cn

Received 26 October 2016; Revised 15 January 2017; Accepted 1 March 2017; Published 22 March 2017

Academic Editor: Nicolas Gourdain

Copyright © 2017 Wei Li et al. This is an open access article distributed under the Creative Commons Attribution License, which permits unrestricted use, distribution, and reproduction in any medium, provided the original work is properly cited.

Changing the blade outlet width is an important method to adjust the performance curves of centrifugal pumps. In this study, three impellers with different blade outlet widths in an engine cooling water pump (ECWP) were numerically simulated based on ANSYS-CFX software. Numerical calculation reliability was validated based on the comparison between simulation results and experimental datum. As the blade outlet width increases, from the performance curves, the investigated ECWP head increases gradually; and the best efficiency point (BEP) offsets to larger flow rate; and the high efficiency region (HER) is becoming larger; and the critical cavitation pressure of the investigated ECWP at BEP increases, which indicates that the cavitation performance at BEP became worse. Compared with the internal flow field, we find vortex appears mainly in the blade passage near the tongue and volute outlet, and the region of the low static pressure is located in the blade inlet suction surface, and impeller inlet and outlet are the regions of high turbulence kinetic energy. Meanwhile, at the same flow rate, with the increase of blade outlet width, the areas of vortex and low static pressure become obvious and bigger.

1. Introduction

The engine cooling water pump (ECWP) is an important part in the motor and engine, and it has been widely used for circulating cooling water and carrying the heat away from the engine parts. Compared with conventional centrifugal pumps, ECWP is always working in the environment with the high temperature, changed rotational speed, and the restricted dimension space, which leads to its poor cavitation performance and finally shortens the reliability and life of the cooling system. So, some effects have been devoted so far to study the cavitation performance of ECWP. Shi et al. [1, 2] did structure improvement and optimization of automobile pump based on numerical simulation with opened centrifugal impeller. Li et al. [3, 4] predicted cavitation performance of ECWP and proposed the optimal design of impeller that can improve the cavitation performance. Discussion on the pump cavitation in LJ465Q series engine was made by Liao and Xie [5]. Some improvement is proposed by Liu et al. [2] in a vehicle pump such as decreasing the blade angle at trailing edge, expanding the cross section of the outlet pipe, and gradually increasing the depth of the volute along the flow direction to improve the performance of pump.

Outlet width, one of the main geometric parameters of the impeller, has an important influence on hydraulic and cavitation performance of centrifugal pumps. Shi et al. [6] carried out the numerical and experimental study on a deep-well centrifugal pump with four different impeller outlet widths. The results show that single stage head and single stage power both increased and BEP offset to larger flow rate with the increase of impeller outlet width. The results of performance indicate that the oversize impeller outlet width will lead to poor pump performance and will increase shaft power. Song et al. [7] investigated the cavitation behavior in impeller with different blade profiles and found that it has a key effect on the development of sheet cavitation in impeller and also influences the distribution of sheet cavitation in impeller channels. Zhang et al. [8] analyzed the impact on the cavitation performance for centrifugal pumps by changing the blade leading edge shape. The results show that the leading edge extending forward along the shroud can

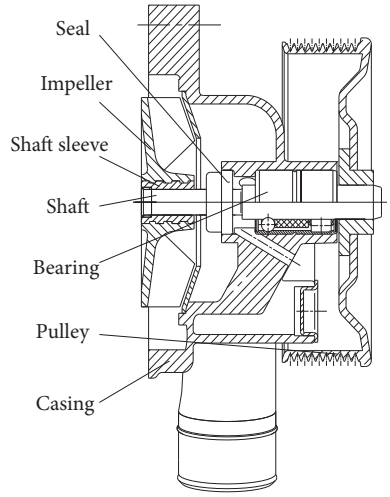

Figure 1: Centrifugal structure of ECWP.

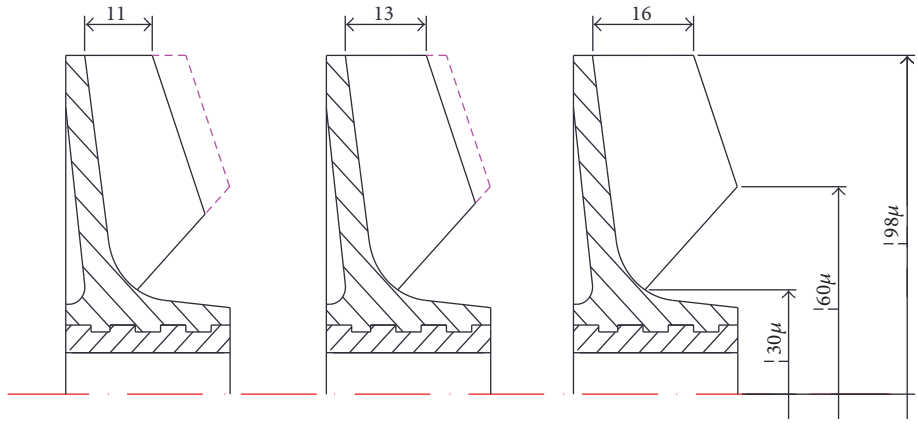

Figure 2: Impeller cross section with three different blade outlet widths.

improve the inlet flow condition and cavitation performance. But the cavitation performance has been reduced immensely when the leading edge extends backward along the shroud. Liu et al. [9, 10] had done some work about the effects of impeller outlet width on the performance in two side chambers of a centrifugal pump. However, the report about the effect of cavitation performance by changing the blade outlet width is extremely lacking.

In this work, the hydraulic and cavitation performance and the internal flow of ECWP were researched with three different blade outlet widths of impeller. By changing outlet widths of impeller and keeping other parameters constant, three impellers are obtained and were numerically simulated based on ANSYS-CFX software. In addition, fluid static pressure, turbulent kinetic energy distribution, and vapor volume fraction contours of impeller were observed to analyze the influence of blade outlet width on hydraulic and cavitation performance. This work provides a reference for the performance optimization of ECWP.

2. Geometric Model

2.1. Structure Chart. Considering the special requirements of cylinder structure, process, and engine, the design method of ECWP is different from traditional centrifugal pump. The characteristics of ECWP impeller are as follows: semiopen structure, wide outlet width, ring cross section of suction chamber, rectangular volute cross section, and being driven by pulley. The typical structure of ECWP is shown in Figure 1.

2.2. Impeller Design. The temperature of ECWP in this work is set as 85°C ± 2°C; the main geometric parameters of impeller at the design condition are shown in Table 1.

In order to study the influence of different impeller blade outlet widths, three impeller models were built with three different outlet widths (b_2 = 11 mm, 13 mm, and 16 mm, resp.). Figure 2 shows the impeller cross section with different outlet widths. Figure 3 shows three-dimensional plot of impeller.

Table 1: Impeller parameters of ECWP.

Description	Parameter	Value
Design flow rate (L/min)	Q_{des}	340
Head (m)	H	15
Rotational speed (r/min)	n	3700
Outlet width of impeller (mm)	b_2	16
Inlet angle of blade (°)	α_1	19
Outlet angle of blade (°)	α_2	30
Wrap angle of blade (°)	α	65
Number of blades	Z	7
Inlet diameter of impeller (mm)	d_1	60
Outlet diameter of impeller (mm)	d_2	98

Figure 3: Three-dimensional plot of impeller.

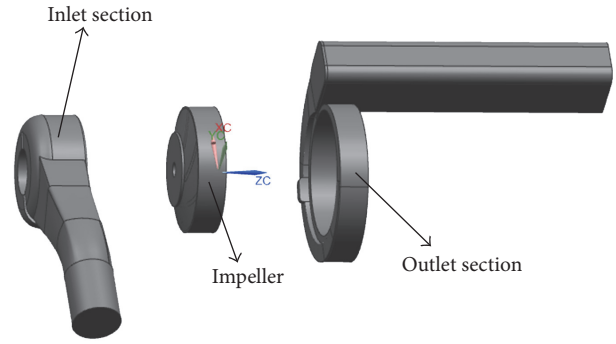

Figure 4: The domains of ECWP.

3. Numerical Simulation

3.1. Calculation Model. The computational domains include three parts: inlet section, outlet section, and impeller. All these parts are completed in the Unigraphics NX software and are shown in Figure 4. The calculation is performed on a Dell workstation with 2 processors (Windows 7 Professional, Inter(R) Xeon(R) CPU, 64 bit, 3.33 GHz, and 48 GB RAM). Considering the uncertainty about the empirical coefficients of cavitation condensation and vaporization and maximum density ratio at the high temperature, which can influence the compressibility characteristics in the cavitation area and the mass transfer between liquid and vapor [11], cavitation numerical simulations at high temperature have a frustrating convergence and lack of reliability. So, combined with the simulation applicability and accuracy, the multiphase flow was numerically simulated in ECWP under 25°C temperature.

3.2. Mesh Analysis. The whole generation process of mesh is carried out in ANSYS-ICEM software, structure mesh was applied in computational domains mesh, and the impeller domain is refined. The mesh configuration of whole flow field is shown in Figure 5, specially the mesh at blade inlet and volute tongue. The mesh can be calculated in ANSYS-CFX fluently, and the value of y^+ is limited under 100 and was in accordance with the turbulence model which was chosen as follows.

3.3. Turbulence Model. In the condition of single phase, turbulence models describe the effects of turbulent fluctuations of velocities and scalar quantities; no turbulence model can get satisfactory results for all applications. So, four turbulence models, namely, RNG k-Epsilon model, k-Epsilon model, k-Omega model, and the shear stress transport model (SST model), are selected to simulate the internal performance of impeller with 16 mm outlet width at standard running conditions (Q_{des} = 340 L/min). By comparing numerical results and the experimental one, it can be found in Table 2 that SST model is the best one that consists of experimental results. So SST turbulence model is the most suitable model for hydraulic performance simulation.

Moreover, in the condition of multiphase flows, the quantity of terms that need to be modeled in momentum equation is many, which makes the modeling of turbulence in multiphase simulations extremely complex [12]. So, SST turbulence model is chosen directly as the turbulent model for cavitation simulation.

3.4. Governing Equations and Discretization. Three steady numerical simulations are conducted employing the time averaged Navier-Stokes equation and the SST turbulent model in ANSYS-CFX software. The Navier-Stokes equation is solved by two-order accuracy upwind scheme and the fully implicit coupling algorithm based on finite volume method in ANSYS-CFX software. The advection terms are in high-resolution format and its convergence accuracy is set as 10^{-4}.

3.5. Mesh Independence Analysis. To reduce computation time and improve accuracy, the optimum quantity of mesh elements in the simulation has been investigated. Also, head was used as the evaluation indexes to judge mesh size. Finally, the least quantity of dependent mesh elements has been obtained when head is obtained with negligible change. Figure 6 shows the dependency of results by comparing external characteristic with different element quantity at 340 L·min^{-1} flow rate (Q).

Table 2: Numerical results with different turbulence models.

Turbulence model	RNG k-Epsilon	k-Epsilon	k-Omega	SST	Experiment
η/(%)	52.11	55.66	54.03	51.36	49.98
H/(m)	17.03	17.41	17.76	16.67	16.35

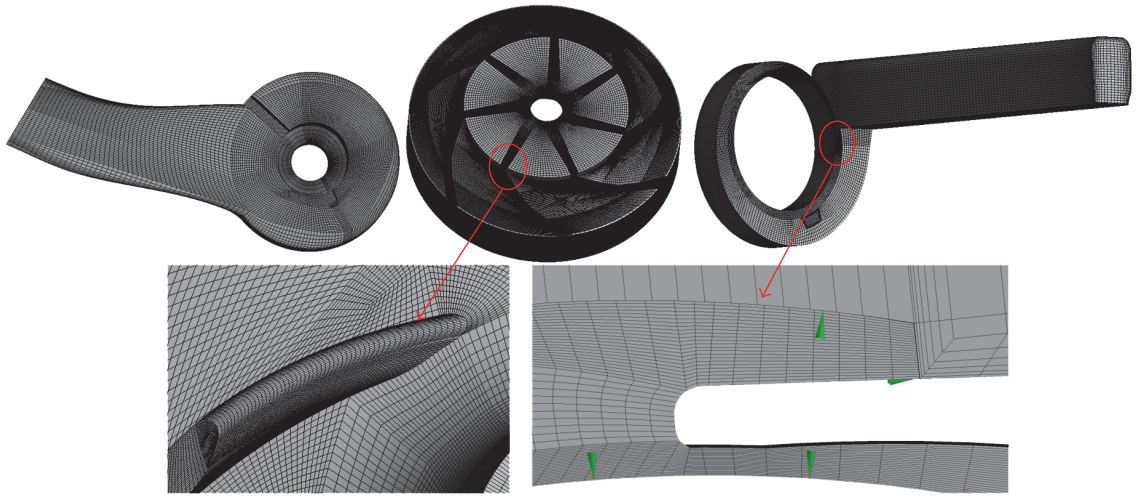

Figure 5: Sketch of whole flow field mesh and the refined mesh of blade inlet and volute tongue.

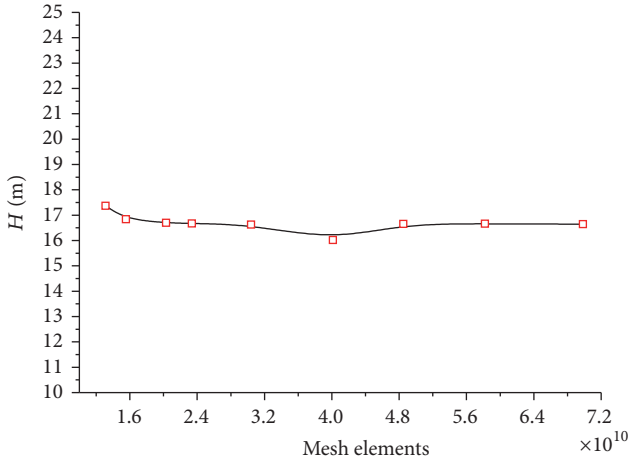

Figure 6: Comparison of the head with different mesh elements.

The quantity of mesh elements is the sum of elements in impeller, inlet pipe, and outlet pipe. Considering the computational ability of computer workstation used in this work, the total mesh number of the mesh is about 2.4 million. As demonstrated in Figure 6, when the quantity of mesh element is about 2.4 million, the change of head is less than 2%, which indicates the convergence of mesh.

Table 3 shows mesh quantity of the whole domains in different parts of pump.

3.6. Cavitation Model. The cavitation model is based on the assumption that the water and vapor mixture in the flow can be perceived as a homogeneous fluid. Cavitation model is the mathematical model used to describe the transformation between vapor phase and liquid phase. In this study, the Zwart-Gerber-Belamri cavitation model [13] based on Rayleigh-Plesset Equation in the transport equation model was selected. The full phase mass per unit volume transmission rate and void volume change rate are defined as follows:

Table 3: Information of whole mesh statistics.

Components	Inlet section	Impeller	Outlet section
Quantity of mesh elements	299970	1685215	353175
Minimum orthogonal angle/°	15.8	36.4	32.9

$$\dot{m}_{fg} = F\frac{3r_{nuc}\left(1-r_g\right)\rho_g}{R_B}\left(\frac{2}{3}\frac{\left|p_v-p\right|}{\rho_f}\right)^{1/2}\operatorname{sgn}\left(p_v-p\right), \quad (1)$$

$$\frac{\mathrm{d}V_B}{\mathrm{d}t} = \frac{\mathrm{d}}{\mathrm{d}t}\left(\frac{4}{3}\pi R_B^3\right) = 4\pi R_B^2\left(\frac{2}{3}\frac{p_v-p}{\rho g}\right)^{1/2},$$

where F is an empirical coefficient, R_B represents the bubble radius, $r_{nuc} = 5\times10^{-4}$, $r_g = 1\times10^{-6}$, p_v is the vaporization pressure and p is the pressure of the liquid around the bubble, V_B is bubble volume.

3.7. Boundary Conditions. The numerical simulation flow domains are divided into two types: stationary reference frame and rotating reference frame. And inlet section and outlet section belong to the former while impeller is situated in the latter. The interface between the stationary reference

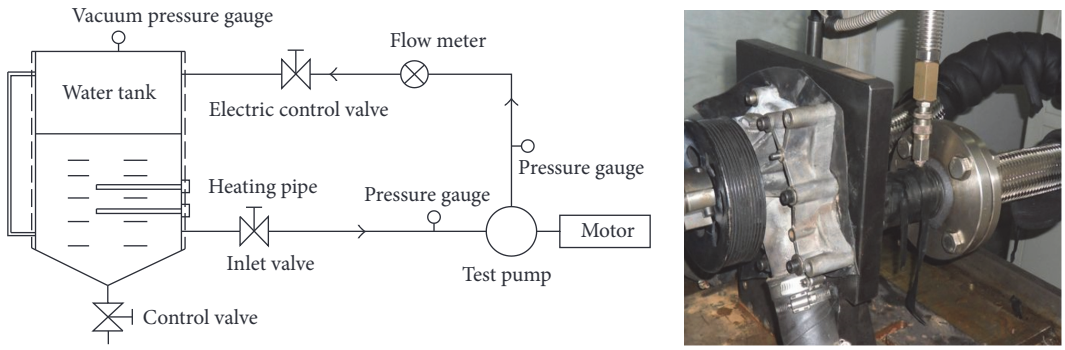

Figure 7: Closed experiment rig of ECWP.

frame and the rotating one is set as frozen rotor. The specified pitch angles are set as 360° and general grid interface (GGI) model is chosen to process data transmission between the stationary and the rotating reference frame. The inlet boundary is set as absolute total pressure based on the zero reference absolute pressure while the outlet boundary was set as mass flow rate. The wall roughness is set as 12.5 μm, and the standard wall function is chosen in the domain near the wall and the wall no-slip boundary condition is set as adiabatic wall. Meanwhile, the volume fraction of water in inlet and bubble volume fraction is set as 1 and 0, respectively.

In the simulation of the cavitation performance, the occurrence degree of cavitation was controlled by adjusting the inlet total pressure, the average bubble radius is set as 2×10^{-6} mm, and the vaporization pressure p_v is set as 3574 Pa. In the simulation of the external characteristics, the mass flow rate is controlled by changing outlet boundary condition, and the other parameters are kept identical.

4. Experimental Verification

4.1. Experimental Rigs and Methods. The closed performance experiment rig of ECWP (shown in Figure 7) is set up to verify the accuracy of the numerical simulation, which precedes the requirements of national standard (GB 3216-89, GB 1882-80, and QCT 288.2-2001). The accuracy of the experiment system is ±0.5%.

The experiment is performed according to ISO 9906 which is the international experiment standard for pumps. The experimental method and some facilities are the same as the reference [14]. The main technical parameters of the experiment bed are as follows: rotational speed $n \leq 8000$ r/min, water temperature $T \leq 120$°C, and flow rate $Q \leq 400$ L/min. Meanwhile, the inlet and outlet pressure are measured separately by two pressure transmitters that the error of measurement is less than 0.15%, while the temperature is controlled by PID (Proportion Integral Derivative) system. Besides, in order to draw the hydraulic performance curves, the outlet flow rate is adjusted to change the working condition. The flow rate is kept at the Q-BEP (340 L/min) and the rotational speed is set as 3700 r/min; then the inlet pressure is reduced slowly to stimulate the cavitation inception in the cavitation experiment.

In the pump performance experiment, net positive suction head (NPSH) is defined as follows:

$$\mathrm{NPSH} = \frac{p_s}{\rho g} + \frac{{v_s}^2}{2g} - \frac{p_v}{\rho g}, \tag{2}$$

where NPSH is the net positive suction head, m; p_s is the total pressure of pump inlet, Pa; v_s is the absolute velocity at inlet, m/s; p_v is the vaporization pressure for liquid, Pa; ρ is the destiny of water, $\rho = 1000\,\mathrm{kg/m^3}$; g is the gravitational acceleration ratio, $g = 9.8\,\mathrm{m/s^{-2}}$.

4.2. Experimental Results and Analysis. According to the designed three-dimensional model, ECWP experimental model ($b_2 = 16$ mm) was processed into products and then sent to have the hydraulic performance experiment. The hydraulic performance experiment was carried out with 3700 r/min rotational speed and 25°C temperature. To generate cavitation performance, the inlet total pressure is varied progressively by changing the valve opening, while keeping the flow rate and rotational speed remaining 340 L/min and 3700 r/min, respectively. The hydraulic and cavitation characteristic curves obtained by experimental and numerical simulation were both shown in Figure 8.

It can be seen from Figure 8 that the change trend in numerical simulation result is consistent with that in experimental result of both hydraulic and cavitation performance. Besides, efficiency, head, and NPSH of numerical simulation are all slightly higher than that of experiment. To be specific, the pump simulation efficiency is about 2.8% higher and the head is about 2% higher than that of experiment at BEP. NPSH is also about 0.33 m higher than that of experiment at 3700 r/min rotational speed and 340 L/min flow rate. To sum up, the reliability of numerical simulation is verified by comparing the results between experiment and numerical simulation, which indicates that the numerical calculation is the effective method to predict the hydraulic and cavitation performance of centrifugal pumps.

5. Simulation Results and Discussions

5.1. Hydraulic Performance. Hydraulic performance of ECWP with different blade outlet widths is obtained by

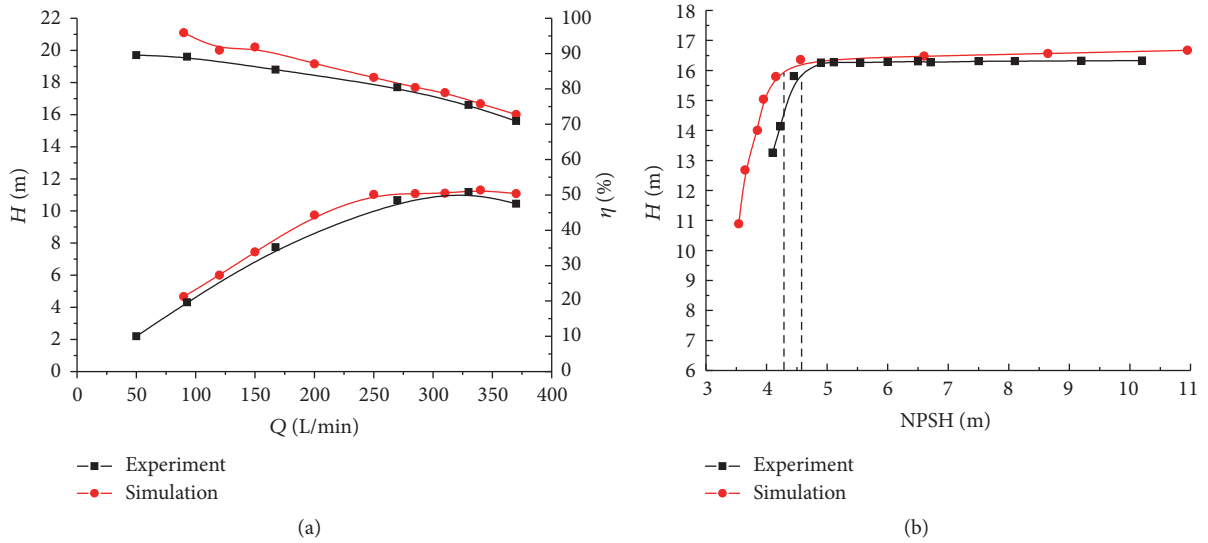

Figure 8: Comparison with hydraulic (a) and cavitation (b) performance.

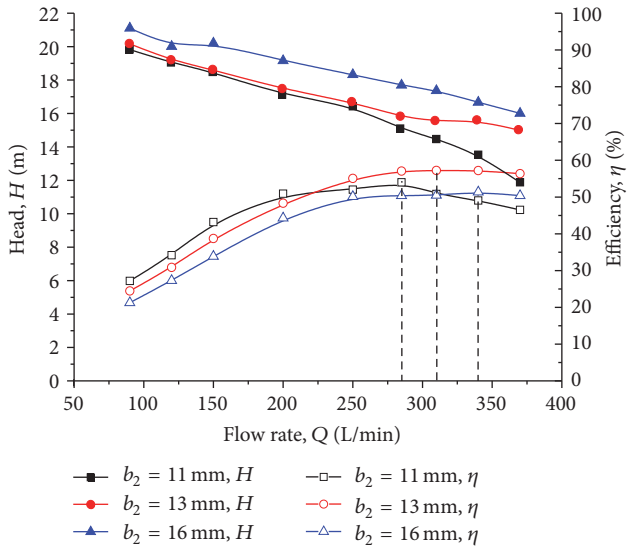

Figure 9: Hydraulic performance with different blade outlet widths.

numerical simulation. The head and efficiency are shown in Figure 9.

According to the performance curves, it can be found that head increases gradually along with the increase of blade outlet width. The head function (6) can be obtained based on the velocity triangle about blade outlet width with the same flow rate. Also, its first derivative function is more than zero, so it is an increasing function. Therefore, head will increase when blade outlet width becomes larger.

$$H = \frac{u_2 v_{u2} - u_1 v_{u1}}{g}, \tag{3}$$

$$v_{u2} = u_2 - \frac{v_{m2}}{\tan \beta}, \tag{4}$$

Table 4: Flow rate and efficiency at BEP.

Blade outlet width/(mm)	11	13	16
Q/(L/min)	285	310	340
η/(%)	54.1	57.2	51.36

$$v_{m2} = \frac{Q}{\pi D_2 b_2 \psi_m}, \tag{5}$$

$$H = \left(\frac{{u_2}^2 - u_1 v_{u1}}{g}\right) - \left(\frac{Q u_2}{g \pi D_2 b_2 \tan \beta}\right) \frac{1}{b_2} = A - \frac{B}{b_2} \quad (A, B > 0). \tag{6}$$

Table 4 is the flow rate and pump efficiency at BEP with different blade outlet widths. When blade outlet width changes from 11 mm and 13 mm to 16 mm, BEP offsets to larger flow rate. Similar observation was also found in [6]. The flow rate at BEP increased 8.77% and 9.68%, respectively. Also there are some differences of efficiency in three cases at BEP. Meanwhile, with the blade outlet widths increases, the high efficiency region (HEG) of ECWP is becoming larger. According to (6), we know that its second derivative function is less than zero. So, it is also a convex function. In other words, head becomes much more sensitive to the change of blade outlet width when blade outlet width becomes larger. And the range of blade outlet width is bigger near BEP.

5.2. Discussion of Internal Flow. The internal flow fields of impeller with three blade outlet widths are simulated at the same flow condition. Figure 10 is the surface streamline in the cross section of impeller with different blade outlet widths. From the pictures, it can be found that the vortices appeared mainly in two areas: blade passage near tongue and volute outlet. And with the blade outlet width increases, the vortex at volute outlet becomes much more obvious and bigger, which

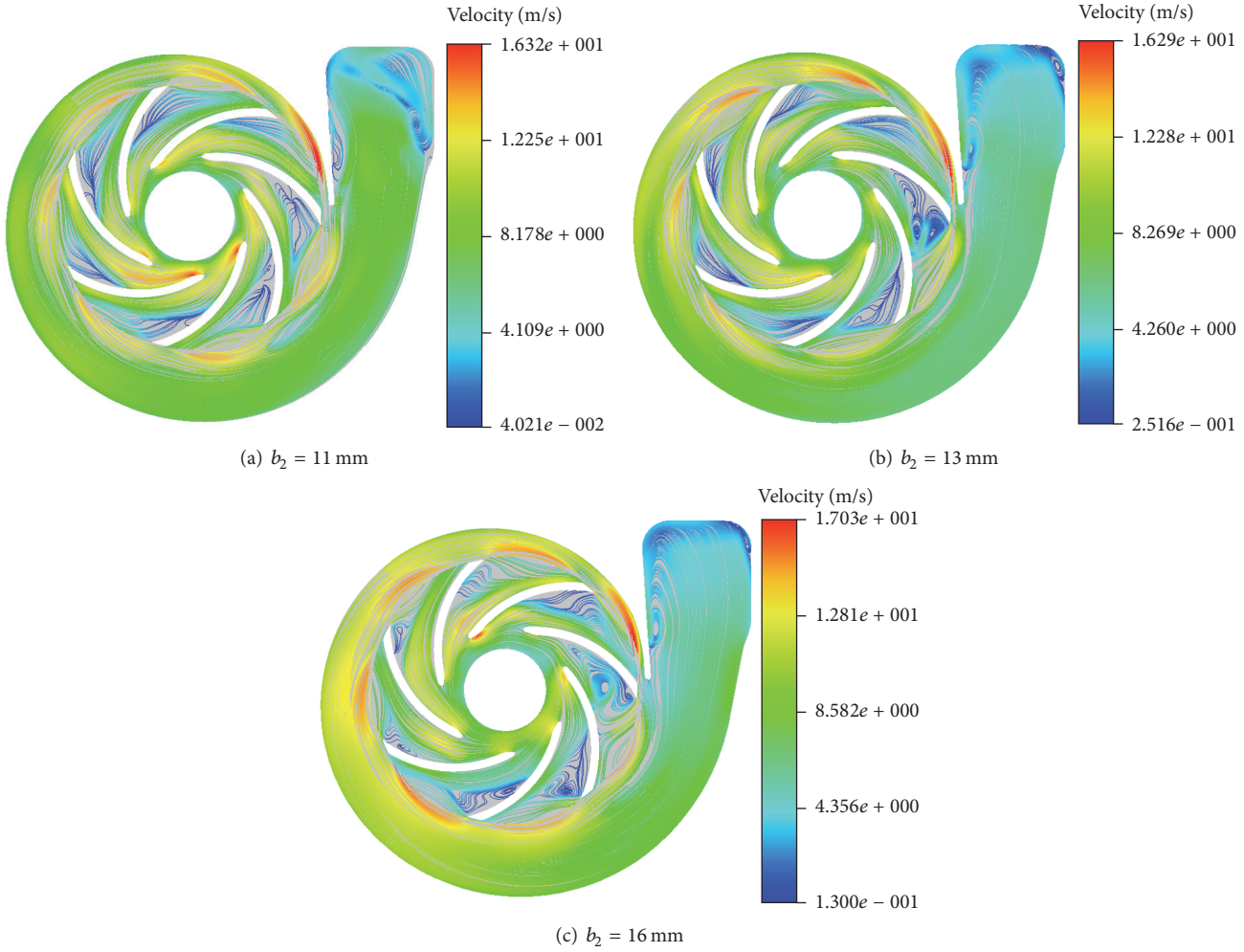

(a) $b_2 = 11$ mm (b) $b_2 = 13$ mm (c) $b_2 = 16$ mm

FIGURE 10: Surface streamline in the cross section.

has also been reported in [15]. As a result of the interaction flow fields between impeller and tongue, which can be seen from Figures 10(b) and 10(c), some obvious vortices occurred in the blade passage near tongue and will cause more losses.

The static pressure distributions with different blade outlet widths in the cross section of impeller are compared in Figure 11. It can be seen from the figure that the high pressure area always appears at the surface of blade outlet pressure. And also, in the blade inlet suction surface, the low static pressure region can be observed. With the increasing of the outlet width, the low pressure areas become bigger which is consistent with the research results in [16]. And the pressure value is lower at the impeller blade inlet suction surface. When the outlet width changes from 11 mm to 16 mm, the maximum value of the static pressure increases from 267.2 kpa to 270.9 kpa, while the minimum value of the static pressure increases from −9.85 kpa to −6.20 kpa. And the differential pressure becomes bigger with the increase of impeller blade outlet width.

Also, the pressure distributions of the cross section with different blade outlet widths at BEP are shown in Figure 12. It can be found from Figure 12 that the pressure distribution of the cross section at the blade inlet is quite different. When the blade outlet width is 16 mm, the low pressure zone is much wider than that of the others. The pressure distribution in the back chamber is similar to each other and the static pressure increases gradually along the longitudinal direction. From the above analysis it can be found that great change happens at the blade inlet which would have influence on the cavitation performance.

The turbulence kinetic energy contours in the cross section of impeller are shown in Figure 13. It can be found obviously that high turbulence kinetic energy exists in the regions of impeller inlet and outlet. Particularly, from Figures 13(b) and 13(c), high turbulence kinetic energy can be found from the blade passage near volute tongue; from Figures 10(b) and 10(c), disorganized surface streamline can be found. And both indicate that violent vortex and much more losses exist in the blade passage near the volute tongue [17, 18]. When the outlet width changes from 11 mm to 16 mm, the maximum value of turbulence kinetic energy increases from 1.247 m^2/s^2 to 1.619 m^2/s^2, while the minimum value of the turbulence kinetic energy increases from 0.002375 m^2/s^2 to 0.002846 m^2/s^2.

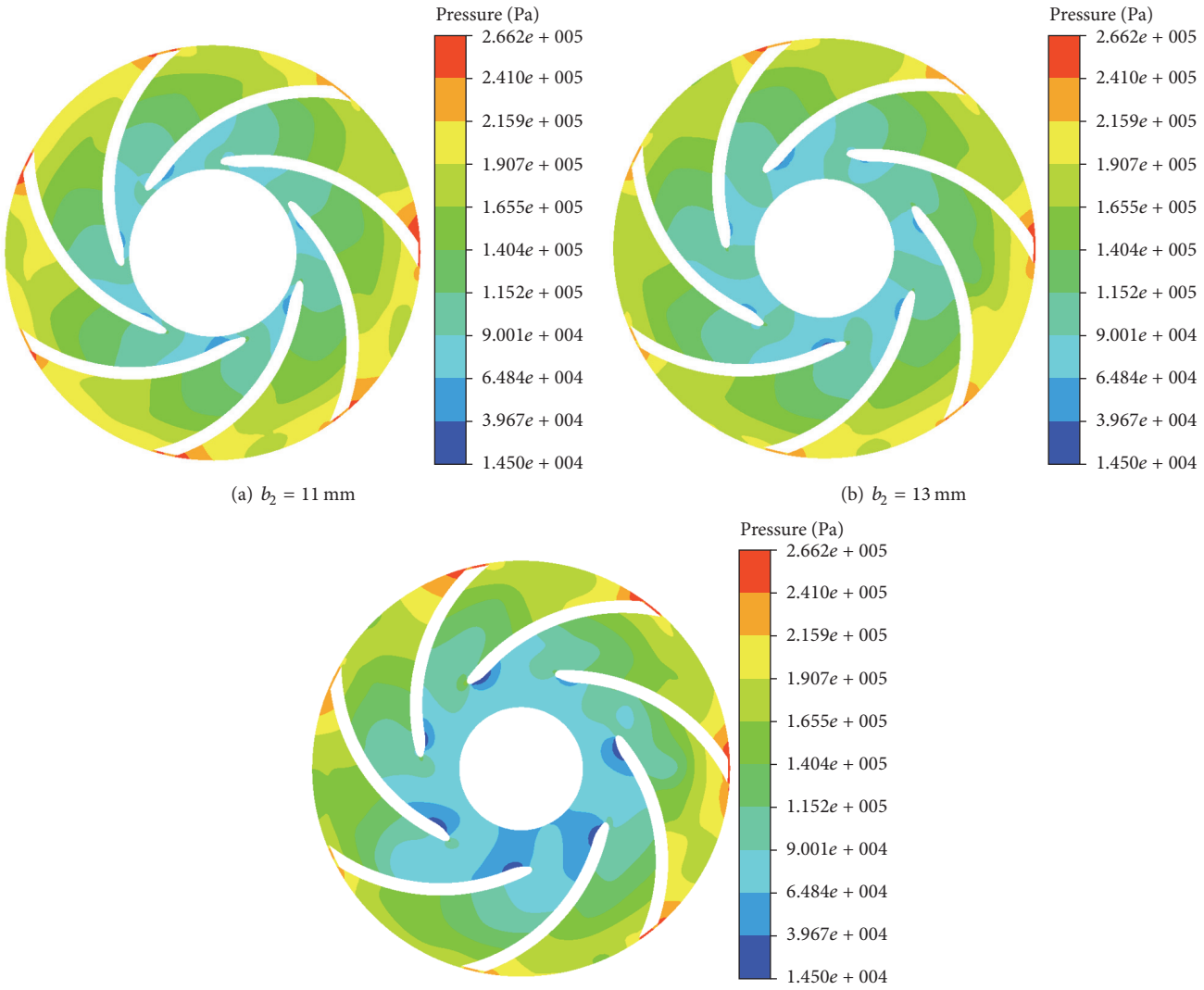

Figure 11: Static pressure distribution in the cross section.

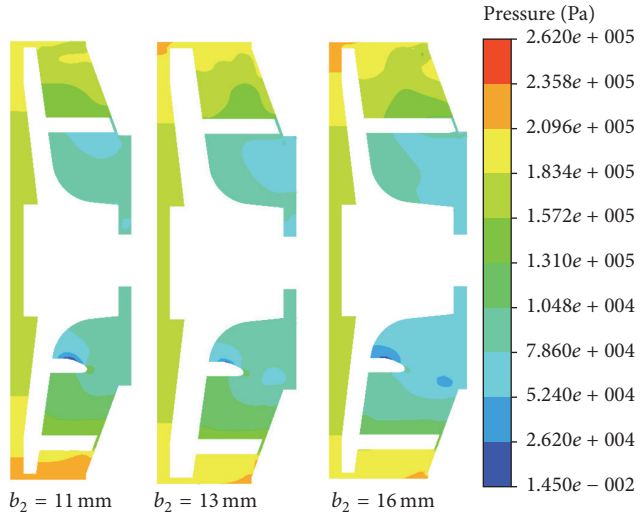

Figure 12: Pressure distribution between the pump casing and impeller hub.

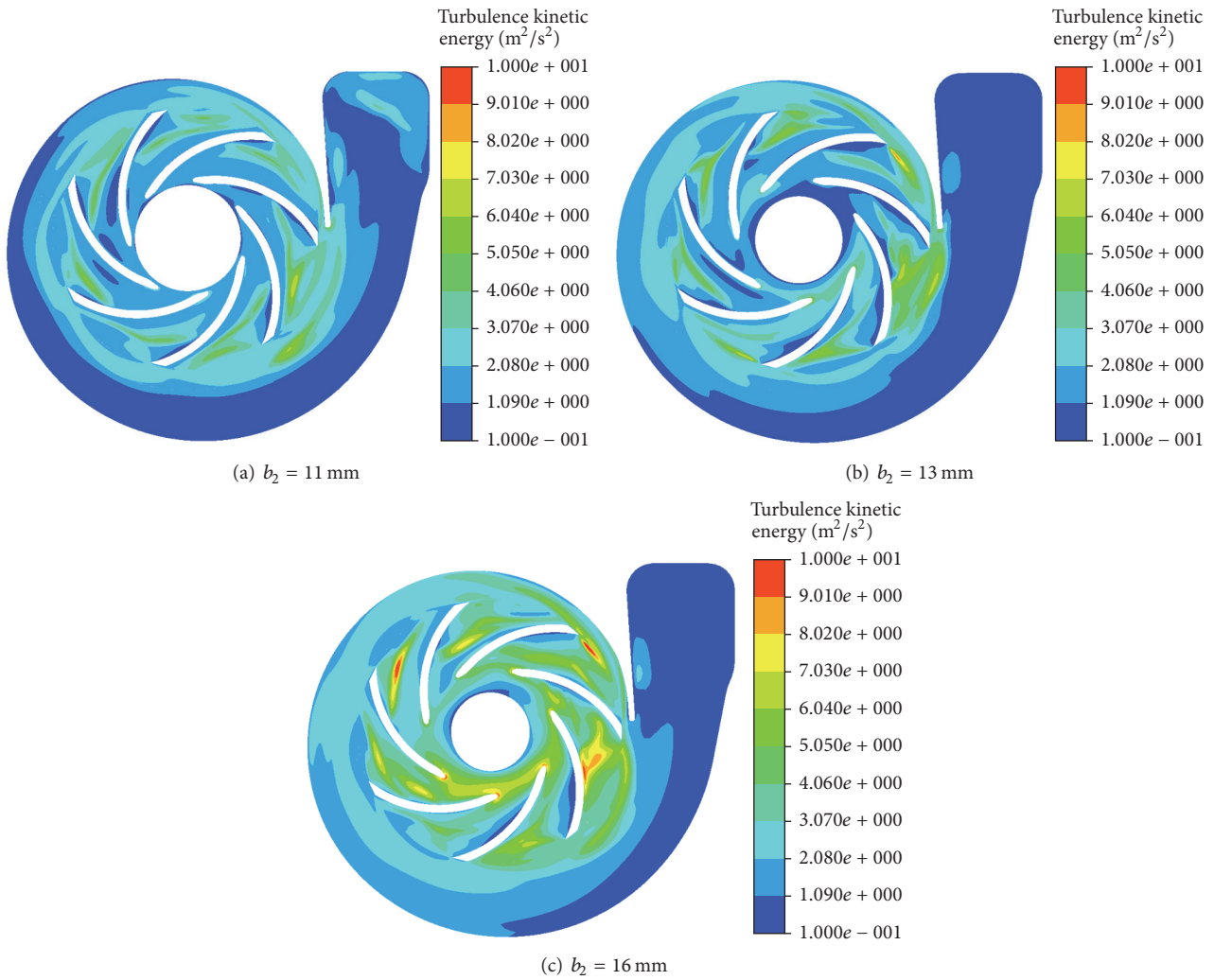

Figure 13: Turbulence kinetic energy contours in the cross section.

5.3. Cavitation Performance at BEP. The cavitation performance at BEP with different blade outlet widths is numerically simulated and is shown in Figure 14. The results indicate that the cavitation in ECWP has a significant influence on head, especially in the period of cavitation development, which always causes a large loss of head.

From the cavitation performance, the critical point of cavitation is marked by the NPSH at which the head has fallen by 3%. The critical cavitation pressure increases with the increase of blade outlet width. It can be seen from Figure 14 that when blade outlet width is 11 mm, 13 mm, and 16 mm, the critical cavitation pressure is, respectively, about 33.7 kPa, 35.4 kPa, and 37.8 kPa; among them 11 mm outlet width has the smallest critical cavitation pressure. That is to say, cavitation performance of the 11 mm impeller is the optimal one. The analysis results are also consistent with the conclusion that BEP offsets to larger flow rate, because cavitation of centrifugal pump becomes worse at the high flow rate conditions.

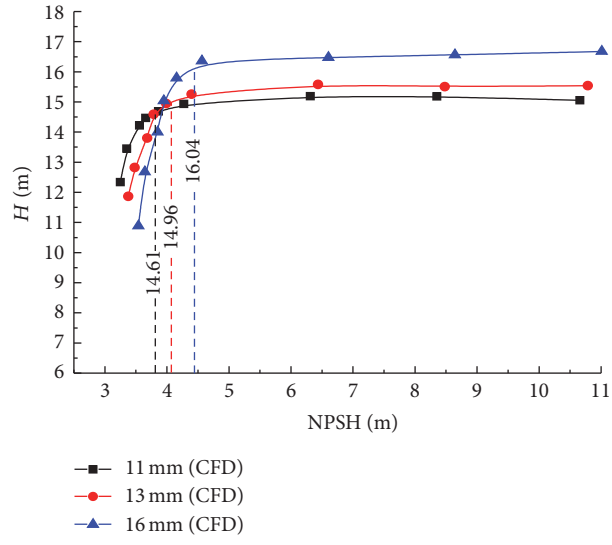

Figure 14: Cavitation performance with different blade outlet widths at BEP.

b_2 = 11 mm (35.4 kPa) b_2 = 13 mm (35.4 kPa) b_2 = 16 mm (35.4 kPa)

Figure 15: 10% bubble volume concentration distribution of the three impeller models.

5.4. Bubble Volume Distribution at BEP. Bubbles, the direct product of cavitation, are broken suddenly after moving into the high pressure areas, which will cause cavitation damage such as shortening the ECWP reliability and producing vibration and noise. Figure 15 shows 10% bubble volume concentration distribution of three pump models with different blade outlet widths at the same inlet total pressure.

From Figure 15, it can be found that the bubble volume concentration in impeller gradually increases with the increase of the blade outlet width. Furthermore, 11 mm impeller has the latest experiment and smallest bubble area, which proves that the cavitation performance of the impeller with 11 mm impeller is better than others, and the analysis results are also consistent with the cavitation performance curves.

6. Conclusion

In this study, the numerical calculation reliability is validated, which indicates that the numerical calculation is the effective method to predict the hydraulic and cavitation performance of centrifugal pumps.

It is an important way to adjust the performance curves of centrifugal pump by changing the blade outlet width. With the increase of blade outlet width, head of ECWP increases gradually, and BEP offsets to larger flow rate, and the high efficiency region (HER) is becoming larger, while there is a small change in the efficiency at BEP.

The internal flow in ECWP is extremely complex. Vortex appeared mainly in the blade passage near the tongue and volute outlet; the low static pressure is located in the surface of blade inlet suction, while the high turbulence kinetic energy regions are located in inlet and outlet of impeller. Meanwhile, at the same flow rate, as the blade outlet width increases, the area of vortex and low static pressure becomes obvious and bigger.

The impeller with different blade outlet widths has its own BEP at the same rotational speed. From 11 mm to 13 mm and 16 mm of blade outlet width, the bubble volume concentration in the impeller gradually increases at the same inlet absolute pressure, and the critical cavitation pressure of the investigated ECWP is also increased, which are consistent with the conclusion that BEP offsets to larger flow rate, because cavitation of centrifugal pump becomes worse at the high flow rate conditions.

Conflicts of Interest

The authors declare that there are no conflicts of interest regarding the publication of this paper.

Acknowledgments

This work was supported by the National Natural Science Foundation of China (no. 51409127); PAPD; Six Talents Peak Project of Jiangsu Province (no. HYZB-002); Key Research and Development Projects of Jiangsu Province (nos. BE2015119 and BE2015001-4); the Natural Science Foundation of Jiangsu Province (no. BK20161472); and Scientific Research Start Foundation Project of Jiangsu University (no. 13JDG105).

References

[1] W. Shi, B. Pei, W. Lu, C. Wang, and W. Li, "Optimization of automobile pump based on CFD," *Journal of Drainage and Irrigation Machinery Engineering*, vol. 31, no. 1, pp. 15–19, 2013.

[2] T.-T. Liu, T. Wang, B. Yang, and C.-G. Gu, "Numerical simulation and structure improvement for a car pump with opened centrifugal impeller," *Journal of Engineering Thermophysics*, vol. 30, no. 6, pp. 961–963, 2009.

[3] W. Li, W.-D. Shi, B. Pei, H. Zhang, and W.-G. Lu, "Numerical simulation and improvement on cavitation performance of engine cooling water pump," *Transactions of CSICE*, vol. 31, no. 2, pp. 165–170, 2013.

[4] W. Li, W. Shi, H. Zhang, B. Pei, and W. Lu, "Cavitation performance prediction of engine cooling water pump based on CFD," *Journal of Drainage and Irrigation Machinery Engineering*, vol. 30, no. 2, pp. 176–180, 2012.

[5] N. Liao and D. Xie, "Discussion on the pump cavitation in LJ465Q Series," *Engine Equipment Manufacturing Technology*, vol. 02, pp. 177–179, 2010.

[6] W. Shi, L. Zhou, W. Lu, B. Pei, and T. Lang, "Numerical prediction and performance experiment in a deep-well centrifugal pump with different impeller outlet width," *Chinese Journal of Mechanical Engineering*, vol. 26, no. 1, pp. 46–52, 2013.

[7] P. Song, Y. Zhang, C. Xu, X. Zhou, and J. Zhang, "Numerical studies on cavitation behavior in impeller of centrifugal pump with different blade profiles," *International Journal of Fluid Machinery and Systems*, vol. 8, no. 2, pp. 94–101, 2015.

[8] S. Zhang, R. Zhang, S. Zhang, and J. Yang, "Effect of impeller inlet geometry on cavitation performance of centrifugal pumps based on radial basis function," *International Journal of Rotating Machinery*, vol. 2016, Article ID 6048263, 9 pages, 2016.

[9] H. Liu, Y. Wang, and S. Q. Yuan, "Effects of impeller outlet width on the vibration and noise from centrifugal pumps induced by flow," *Journal of Huazhong University of Science and Technology*, vol. 40, no. 1, pp. 123–127, 2012.

[10] H. Liu, J. Ding, M. Tan, J. Cui, and Y. Wang, "Analysis and experimental of centrifugal pump noise based on outlet width of impeller," *Transactions of the Chinese Society of Agricultural Engineering*, vol. 29, no. 16, pp. 66–73, 2013.

[11] B. Ji, X. Luo, Y. Wu, X. Peng, and Y. Duan, "Numerical analysis of unsteady cavitating turbulent flow and shedding horseshoe vortex structure around a twisted hydrofoil," *International Journal of Multiphase Flow*, vol. 51, pp. 33–43, 2013.

[12] E. Goncalvès and B. Charrière, "Modelling for isothermal cavitation with a four-equation model," *International Journal of Multiphase Flow*, vol. 59, pp. 54–72, 2014.

[13] J. Philip, A. G. G. Zwart, and T. A. Belamri, "Two-phase flow model for predicting cavitation dynamics," in *Proceedings of the International Conference on Multiphase Flow*, Yokohama, Japan, 2004.

[14] T81266.2, *Internal Combustion Engine Cooling Water Pumps Part 2: Assemblies and Test Methods*, China Machine Press, Beijing, China, 2010.

[15] Z. Weihua, *The study of water pump with high efficiency for the motor [Ph.D. thesis]*, Tsinghua University, Beijing, China, 2011.

[16] Z. Tingting, Y. Shouqi, L. Jianrui, Z. Jinfeng, and P. Bing, "Impact of impeller parameters on performance of an automobile cooling pump," *Chinese Journal of Automotive Engineering*, vol. 3, no. 2, pp. 100–105, 2013.

[17] J. F. Gülich, *Centrifugal Pumps*, vol. 5, Springer, Berlin, Germany, 2014.

[18] Y. Z. Chen, Z. Y. Cao, G. Q. Deng, and H. M. Huang, *Pump Handbook*, China Petrochemical, Beijing, China, 3rd edition, 2003.

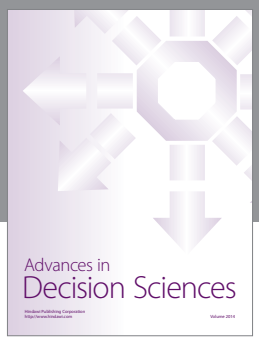

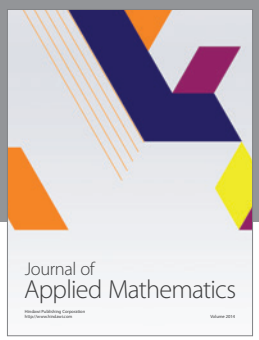

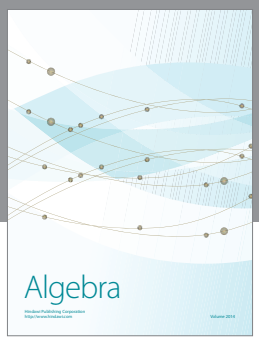

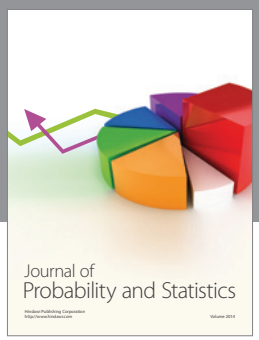

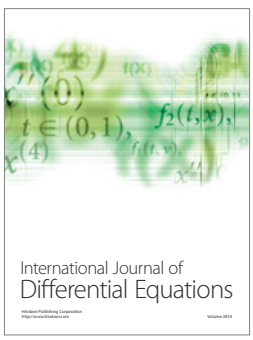

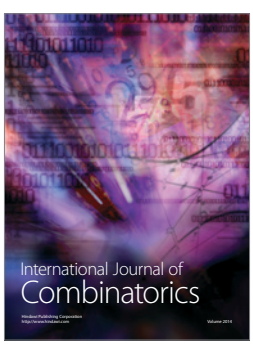

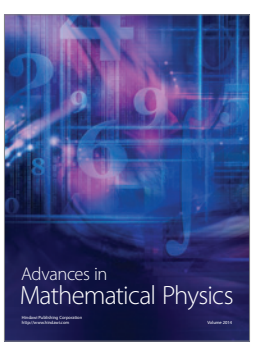

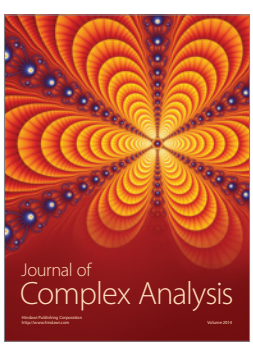

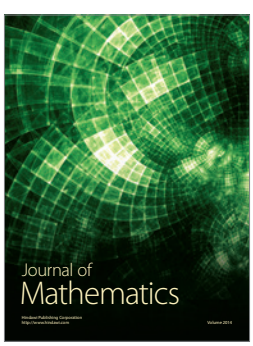

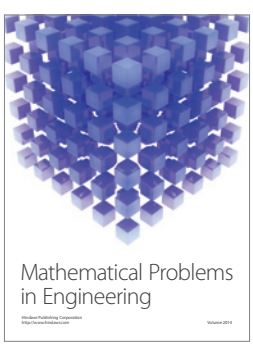

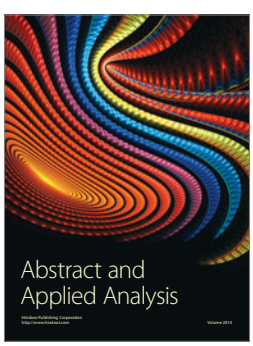

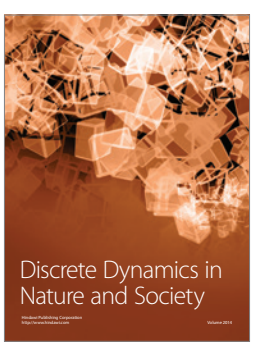

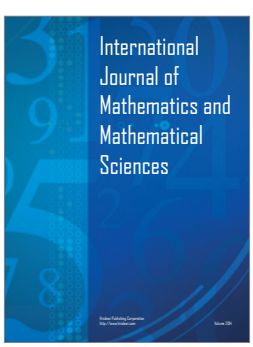

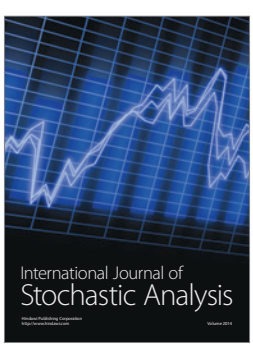

Hindawi

Submit your manuscripts at
https://www.hindawi.com